CHAPTER 4

TETRADENTATE [N_2O_2]-DONOR ASYMMETRIC 'SALEN' TYPE SCHIFF BASE LIGANDS AND THEIR MESOMORPHIC AND PHOTOLUMINESCENT ZINC(II) COMPLEXES

CHAPTER 4

TETRADENTATE $[N_2O_2]$-DONOR ASYMMETRIC 'SALEN' TYPE SCHIFF BASE LIGANDS AND THEIR MESOMORPHIC AND PHOTOLUMINESCENT ZINC(II) COMPLEXES

4.1. Introduction

Transition metal-salen complexes have been a recurrent theme in synthetic co-ordination chemistry, yet interest in this field continue unabated possibly due to their wide applicability being unfolded in recent times.[1-4] A plethora of salen based complexes are now known to act as efficient catalysts both in homogeneous and heterogeneous reactions for asymmetric ring-opening of epoxides, aziridination, cyclopropanation, oxidation, reduction reaction of ketones, epoxidation of olefins, formation of cyclic and linear polycarbonates, catalytic enantio-selective and diastereoselective redox reactions and Diels–Alder reactions.[5–8] Metal salen complexes are also efficient entities to study interactions with DNA leading to the development of sensitive chemical probes for DNA.[9-12] Besides, such systems are also known to exhibit interesting fluorescence,[13-17] magnetic,[17,18] non-linear optical[19-21] and liquid crystalline properties[22–29] and act as electrochemical sensors.[30-32] Metallomesogens based on Zn(II)-salen or π-conjugated Zn(II)-salphen complexes are quite intriguing because of the possibility of combining luminescence with liquid crystallinity to generate newer systems with exotic multifunctional properties.[24,25,33,34] Spacer group modification can lead to substantial change in mesophase as well as photophysical behaviour in such hemi-disc shaped complexes.[24,25,33,34] In past few years we have reported some novel fluorescent liquid crystalline Zn(II)-salphen complexes with different spacer groups showing hexagonal and rectangular/oblique columnar mesomorphism.[33,34] Creating a minor modification at the central aromatic ring (spacer), new symmetry as well as newer organization in the mesophase could be achieved.[33,34]

Zn(II)-salen or salphen complexes and their derivatives also facilitate various structures which may be utilized for sensory materials for detection of alkaloids[35] and nitro aromatics,[36,37] recognition of biologically relevant anions,[38] selective receptors for tertiary amines,[39] self-assembled heteromultimetallics,[40,41] supramolecular box-shaped assemblies,[42,43] molecular templates in catalytic studies,[44,45] dopants for high performance OLEDS[46-48] and the exploration of their unique second-order nonlinear optical properties.[19,20] High Lewis acidity of the co-ordinatively unsaturated Zn^{2+} ion is believed to be the key to such behaviour. Penta-coordinate nature of the Zn^{2+} ion boosted by the rigid geometry of the 'salen' framework facilitates axial binding of donor ligands resulting in substantial variations in the optical absorption behaviour and enhanced fluorescence emission. In the absence of axial ligand, coordinative saturation is achieved through intermolecular Zn···O interactions involving the phenolate oxygen atoms of the salen ligand acquiring a square based pyramidal structure.[49-52]

In view of the multifarious applications of salen based Zn(II) systems, we report herein a new series of Zn(II) complexes of asymmetric 'salen' based N,N′-bis-(4-n-alkoxysalicylidene)-1,2-diaminopropane ligands. Induction of mesomorphism and photoluminescence via coordination to Zn(II) ion has been demonstrated. All the complexes are blue light emitters both in the solid state as well as in solution. The complexes all exhibited aggregate formation in non-coordinating solvents while only monomer is favoured in coordinating solvents.

4.2. Experimental

The strategy implemented for the synthesis of Schiff base ligands, [N,N′-bis-(4-n-alkoxysalicylidene)- l,2-diaminopropane], hereafter abbreviated as **ndap** (n = 12, 14 and 16 is the number of carbon atoms in alkyl chains; dap = 1,2-diaminopropane) and the mononuclear complexes (**Zn-ndap**) has been summarized in **Scheme 4.1**. The ligands were obtained in a two-step procedure. The first step involves alkylation of 2,4-Dihydroxybenzaldehyde, which is then followed by condensation with l,2-diaminopropane in the second step. Zn(II) complexes were accessed from a reaction between the ligands and zinc acetate in 1:1 molar ratio.

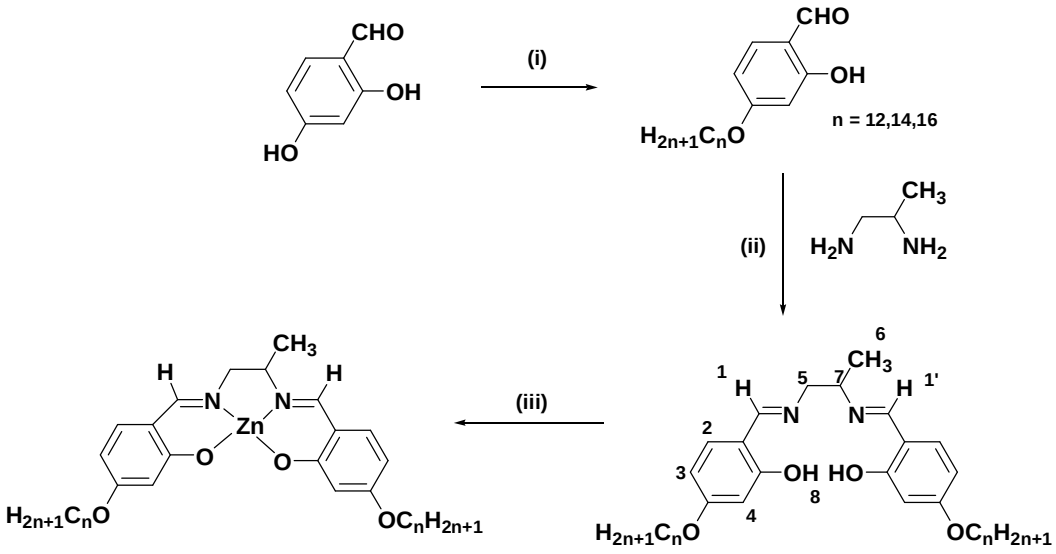

Scheme 4.1: i.$C_nH_{2n+1}Br$, $KHCO_3$, KI, dry acetone, Δ, 24h, and ii. glacial AcOH, absolute EtOH, Δ, 3h iii. $Zn(OAc)_2.2H_2O$, MeOH, stir, 3h.

4.2.1. Synthesis of ligands

Synthesis of n-alkoxysalicyldehyde (n = 12, 14, 16)

2,4-Dihydroxybenzaldehyde (10 mmol, 1.38g), $KHCO_3$ (10 mmol, 1g), KI (catalytic amount) and 1-bromododecane (10 mmol, 2.4g) or 1-bromotetradecane (10 mmol, 2.5g) or 1-bromohexadecane (10 mmol, 2.8g) were mixed in 250 mL of dry acetone and the mixture was heated under reflux for 24 h, and then filtered, while hot, to remove any insoluble solids. Dilute HCl was added to neutralize the warm solution and then extracted with chloroform (100mL). The combined chloroform extract was concentrated to give a purple solid. The solid was purified by column chromatography using a mixture of chloroform and hexane (v/v, 1/1) as eluent. Evaporation of the solvents afforded a white solid product.

Synthesis of N,N'-bis(4-(4'-n-alkoxy)-salicylidene)-1,2-diaminopropane (ndap), n = 12, 14 or 16

General procedure:

Schiff bases (**ndap**) were prepared by adding ethanolic solution of 2-hydroxy-4-(n-alkoxy)salicylaldehyde (1mmol) to ethanolic solution of 1,2-diaminopropane (0.5 mmol).

The solution mixture was heated under reflux with a few drops of acetic acid as catalyst for 3h to yield the light yellow Schiff base, N,N′-bis(4-(4′-n-alkoxy)-salicylidene)-1,2-diaminopropane.The product was collected by filtration and re-crystallized from absolute ethanol to obtain a pure compound.

N, N'-bis(4-(4'-n-dodecyloxy)- salicylidene)-1,2-diaminopropane (12dap)

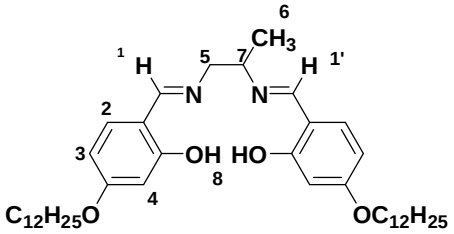

Yield = 0.23g (74%); Anal. Calc. for $C_{41}H_{66}N_2O_4$ (651): C, 75.65; H, 10.22; N, 4.30. Found: C, 75.63; H, 10.21; N, 4.33. %. ^{1}H NMR (400 MHz, $CDCl_3$; Me_4Si at 25°C, ppm): δ = 11.45 (s, 2H, H^8), 8.21 (s, 1H, H^1), 8.17 (s, 1H, $H^{1'}$), 7.01-6.72 (m, 4H, H^2, H^3), 6.21 (s, 2H, H^4), 3.98 (t, $^3J_{H,H}$ = 8Hz, 4H, O-CH_2), 3.70-3.63 (m, 2H, H^5), 1.68 (m, 3H, H^6), 1.35-1.30 (m, 1H, H^7), 1.22-1.03(m,-CH_2 of methylene proton in side chain), 0.89 (t, $^3J_{H,H}$ = 8Hz, 6H, -CH_3). IR (ν_{max}, cm^{-1}, KBr): 3370 (ν_{OH}), 2923 ($\nu_{as(C-H),}$ CH_3), 2857 ($\nu_{s(C-H)}$, CH_3), 1653 ($\nu_{C=N}$), 1227 (ν_{C-O}).

N, N'-bis(4-(4'-n-tetradecyloxy)- salicylidene)-1,2-diaminopropane (14dap)

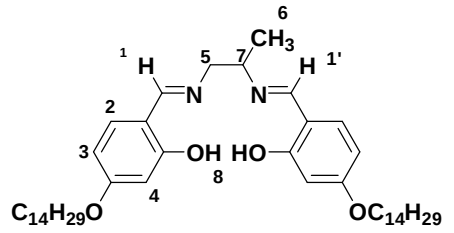

Yield = 0.29g (77%); Anal. Calc. for $C_{45}H_{74}N_2O_4$ (707.1): C, 76.44; H, 10.55; N, 3.96. Found: C, 76.47; H, 10.57; N, 3.95. %. ^{1}H NMR (400 MHz, $CDCl_3$; Me_4Si at 25°C, ppm): δ = 11.43 (s, 2H, H^8), 8.23 (s, 1H, H^1), 8.20 (s, 1H, $H^{1'}$), 7.03-6.75 (m, 4H, H^2, H^3), 6.23 (s, 2H, H^4), 3.98 (t, $^3J_{H,H}$ = 8Hz, 4H, O-CH_2), 3.72-3.65 (m, 2H, H^5), 1.67 (m, 3H, H^6), 1.34-1.27 (m, 1H, H^7), 1.22-1.01 (m,-CH_2 of methylene proton in side chain), 0.89 (t, $^3J_{H,H}$

= 8Hz, 6H, -CH_3). IR (ν_{max}, cm^{-1}, KBr): 3372 (ν_{OH}), 2922 ($\nu_{as(C-H),}$ CH_3), 2854 ($\nu_{s(C-H)}$, CH_3), 1655 ($\nu_{C=N}$), 1225(ν_{C-O}).

N, N'-bis(4-(4'-n-hexadecyloxy)- salicylidene)-1,2-diaminopropane (16dap)

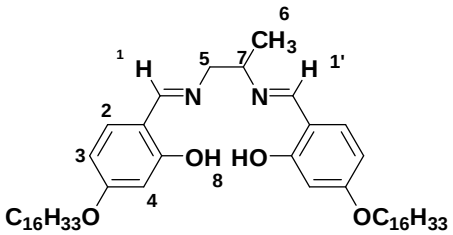

Yield = 0.31g (77%); Anal. Calc. for $C_{49}H_{82}N_2O_4$ (763.2): C, 77.11; H, 10.83; N, 3.67. Found: C, 77.13; H, 10.81; N, 3.70. %. ^{1}H NMR (400 MHz, $CDCl_3$; Me_4Si at 25°C, ppm): δ = 11.47 (s, 2H, H^8), 8.22 (s, 1H, H^1), 8.19 (s, 1H, $H^{1'}$), 7.01-6.74 (m, 4H, H^2, H^3), 6.25 (s, 2H, H^4), 3.98 (t, $^3J_{H,H}$ = 8Hz, 4H, O-CH_2), 3.77-3.58 (m, 2H, H^5), 1.66 (m, 3H, H^6), 1.35-1.28 (m, 1H, H^7), 1.27-1.00 (m,-CH_2 of methylene proton in side chain), 0.88 (t, $^3J_{H,H}$ = 8Hz, 6H, -CH_3). IR (ν_{max}, cm^{-1}, KBr): 3371(ν_{OH}), 2924 ($\nu_{as(C-H),}$ CH_3), 2856 ($\nu_{s(C-H)}$, CH_3), 1654 ($\nu_{C=N}$), 1225 (ν_{C-O}).

4.2.2. Synthesis of zinc (II) complexes (Zn-ndap, n=12, 14, 16)

General procedure:

The ligand **12dap** (0.06g, 0.1mmol) or **14dap** (0.07g.0.1mmol) or **16dap** (0.08g, 0.1mmol) was dissolved in minimum volume of absolute ethanol. To this, an equimolar amount of zinc acetate $Zn(OAc)_2.2H_2O$(0.02g, 0.1mmol) in methanol was then added slowly and stirred for 3h at room temperature. A white solid formed in each case, was filtered, washed with diethyl ether and re-crystallized from chloroform-ethanol (1:1).

Zn-12dap: Yield = 0.05g (75%); Anal. Calc. for $C_{41}H_{64}N_2O_4Zn$ (714.3): C, 68.94; H, 9.03; N, 3.92. Found: C, 68.91; H, 9.07; N, 3.95. %. ^{1}H NMR (400 MHz, $CDCl_3$; Me_4Si at 25°C, ppm): δ = 7.65 (s, 1H, H^1), 7.63 (s, 1H, $H^{1'}$), 6.97-6.70 (m, 4H, H^2, H^3), 6.26 (s, 2H, H^4), 3.99 (t, $^3J_{H,H}$ = 8Hz, 4H, O-CH_2), 3.73-3.67 (m, 2H, H^5), 1.65 (m, 3H, H^6), 1.36-1.31 (m, 1H, H^7), 1.26-0.99 (m,-CH_2 of methylene proton in side chain), 0.88 (t, $^3J_{H,H}$ = 8Hz, 6H, -

CH_3). IR (ν_{max}, cm^{-1}, KBr): 2919 ($\nu_{as(C-H),}$ CH_3), 2853 ($\nu_{s(C-H)}$, CH_3), 1639 ($\nu_{C=N}$), 1215 (ν_{C-O}).

Zn-14dap: Yield = 0.06g (78%); Anal. Calc. for $C_{45}H_{72}N_2O_4Zn$ (770.5): C, 70.15; H, 9.42; N, 3.64. Found: C, 70.14; H, 9.45; N, 3.65. %. ^{1}H NMR (400 MHz, $CDCl_3$; Me_4Si at 25°C, ppm): δ =7.68 (s, 1H, H^1), 7.66 (s, 1H, $H^{1'}$), 6.99-6.71 (m, 4H, H^2, H^3), 6.27 (s, 2H, H^4), 3.99 (t, $^3J_{H,H}$ = 8Hz, 4H, O-CH_2), 3.76-3.60 (m, 2H, H^5), 1.70 (m, 3H, H^6), 1.37-1.26 (m, 1H, H^7), 1.27-1.07 (m,-CH_2 of methylene proton in side chain), 0.89 (t, $^3J_{H,H}$ = 8Hz, 6H, -CH_3). IR (ν_{max}, cm^{-1}, KBr): 2921 ($\nu_{as(C-H),}$ CH_3), 2856 ($\nu_{s(C-H)}$, CH_3), 1639 ($\nu_{C=N}$), 1217(ν_{C-O}).

Zn-16dap: Yield = 0.06g (77%); Anal. Calc. for $C_{49}H_{80}N_2O_4Zn$ (826.6): C, 71.20; H, 9.76; N, 3.39. Found: C, 71.17; H, 9.78; N, 3.40 %. ^{1}H NMR (400 MHz, $CDCl_3$; Me_4Si at 25°C, ppm): δ =7.67 (s, 1H, H^1), 7.64 (s, 1H, $H^{1'}$), 7.00-6.73 (m, 4H, H^2, H^3), 6.22 (s, 2H, H^4), 3.99 (t, $^3J_{H,H}$ = 8Hz, 4H, O-CH_2), 3.74-3.60 (m, 2H, H^5), 1.64 (m, 3H, H^6), 1.34-1.24 (m, 1H, H^7), 1.28-0.98 (m,-CH_2 of methylene proton in side chain), 0.87 (t, $^3J_{H,H}$ = 8Hz, 6H, -CH_3). IR (ν_{max}, cm^{-1}, KBr): 2917 ($\nu_{as(C-H),}$ CH_3), 2854 ($\nu_{s(C-H)}$, CH_3), 1637 ($\nu_{C=N}$), 1215 (ν_{C-O}).

4.3 Results and Discussion

4.3.1. Synthesis and structural assessment

The structure of the ligands(**ndap**) and the corresponding Zn(II) complexes(**Zn-ndap**) were probed by elemental analyses, UV-visible, FT-IR and ^{1}H NMR spectroscopy. A broad band at ~ 3370cm^{-1} attributed to the phenolic -OH group, was observed in the FT-IR spectra of the ligands (ndap). The C=N stretching vibration of the ligands were located in the region of 1653-1655cm^{-1}. Upon complexation, the shift of $\nu_{C=N}$ mode to lower wave number, ~1638cm^{-1}($\Delta\nu \approx 16cm^{-1}$) and absence of ν_{O-H} mode attest to the deprotonation of the Schiff-base prior to coordination of azomethine nitrogen and phenolate oxygen to the Zn^{2+} ion. The ^{1}H NMR spectra of the ligands showed two characteristic signals, at δ = 11.45ppm, corresponding to the OH proton, and at ~8.22 and ~8.18ppm due to the

resonance of two asymmetric imine protons. The ^{1}H NMR spectra of the corresponding Zn(II) complexes did not exhibited any signal for the phenolic –OH proton. Additionally, an up field shift (~0.56ppm) in the peak position of the –N=CH protons further validated azomethine nitrogen coordination.

4.3.2. Liquid crystalline properties

Polarizing optical microscopy and differential scanning calorimetry:

The mesophase behaviour of the compounds has been investigated by polarizing optical microscopy (POM), differential scanning calorimetry (DSC) and variable temperature powder XRD techniques.

Free ligands (**ndap**) are non-mesomorphic presumably owing to greater conformational flexibility. However, upon complexation with Zn(II) metal ion, mesomorphism is induced due to enhanced rigidity of the Schiff base ligand framework. The phase sequence, transition temperatures and associated enthalpies for the Zn(II) complexes are presented in **Table 4.1**. The complexes all exhibited enantiotropic liquid crystalline behaviour. On cooling from the isotropic melt, a grainy texture was observed at 125°C (**Fig. 4.1**). The DSC thermogram of the complexes **Zn-14dap** and **Zn-16dap** (**Fig. 4.2b** and **c**) exhibited two transitions each in the heating and cooling cycle. In the cooling scan, the grainy texture at the mesophase remains unaltered till ambient temperature slowly freezing into a glassy state. For the **Zn-12dap** complex, two additional peaks observed in the heating cycle were ascribed to crystal-crystal transitions (**Fig. 4.2a**). No isotropic liquid-mesophase transition could be detected in the cooling cycle (**Table 4.1**). This might be due to the partial vitrification of the mesophase. Viscous natures of the complexes tend to affect the molecular mobility causing a pronounced hysteresis in the phase transition temperature in all the cases. A gradual decrease in the clearing temperature was observed with increasing number of carbon atoms in the pendant alkoxy arm. The isotropic liquid to mesophase transition temperature also displayed similar trends with increasing chain length. Repeated heating and cooling scans confirmed the reversibility of the thermal behaviour.

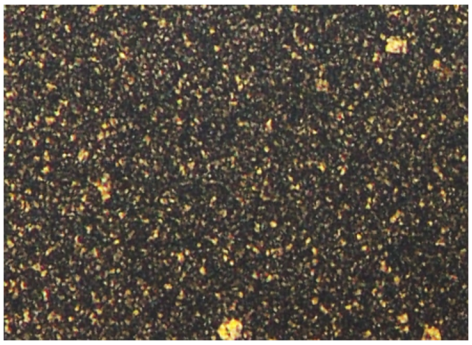

Fig. 4.1: POM image of **Zn-16dap** upon cooling at 125°C.

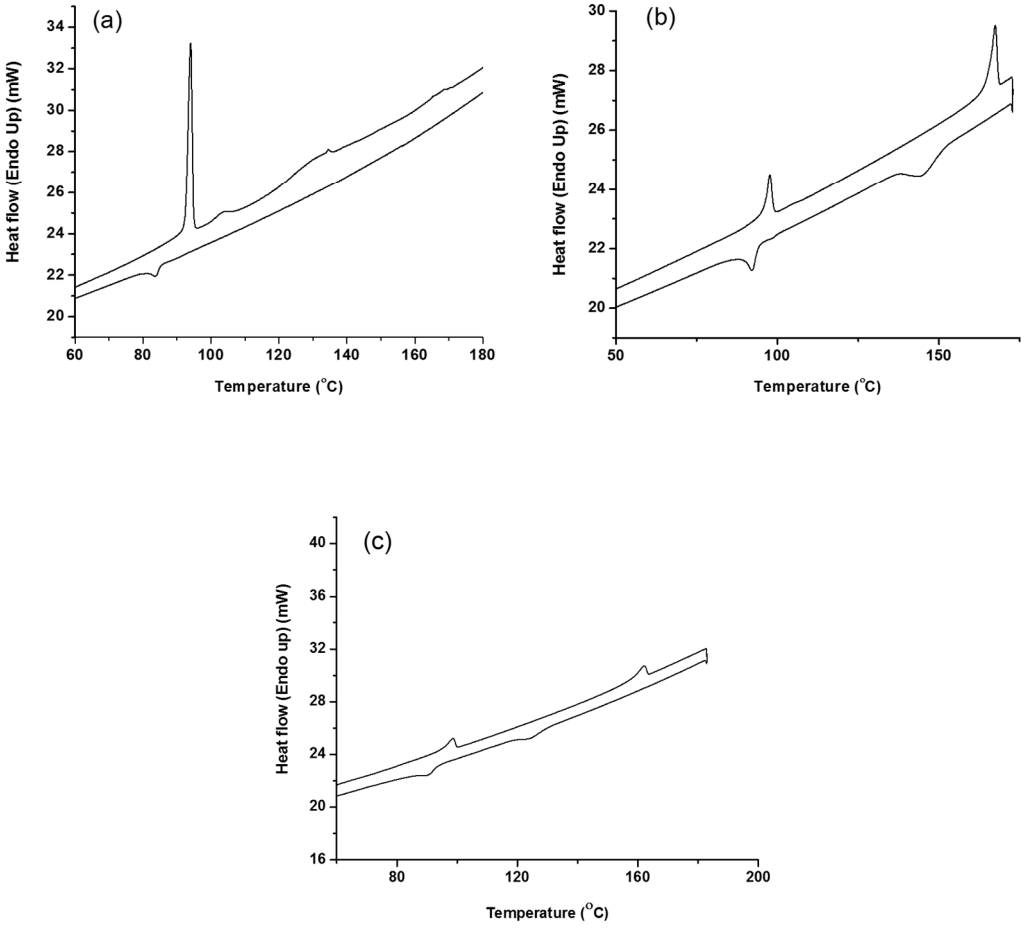

Fig. 4.2: DSC profile of (a) **Zn-12dap**, (b) **Zn-14dap** and (c) **Zn-16dap**.

Table 4.1: Thermodynamic data for the **Zn-ndap** (n = 12, 14, 16) complexes. Transition temperatures are given in °C, and the corresponding enthalpy changes are in parentheses (ΔH; kJ mol^{-1}).

Compounds	Heating[a]	Cooling[a]
Zn-12dap	Cr 94.1(32.8) Cr_1 103.4 (2.4) Cr_2 134.5 (7.9) Col_l 168.6 (1.5) I	I 83.7 (10.1) Cr
Zn-14dap	Cr 97.6 (7.9) Col_l 167.4 (14.1) I	I 144.9(12.2) Col_l 92.2 (6.3) Cr
Zn-16dap	Cr 98.5 (7.0) Col_l 162.1 (8.2) I	I 124.2 (6.2) Col_l 90.3 (5.9) Cr

[a]DSC peak temperature. Cr, Cr_1, Cr_2 refer to phases that are crystalline or solid; Col_l: lamello-columnar phase.

Variable temperature PXRD study

Variable temperature powder XRD study of a representative complex, **Zn-16dap** was carried out both in the mesophase and at room temperature. The X-ray diffraction pattern recorded at 100°C (**Figure 4.3a**, **Table 4.2**) contained several sharp and intense Bragg reflections in the small-angle region and two broad scattering halos (visualized by profile fitting of the data) in the wide-angle region. The broad maxima centered around 4.7 Å and 4.0 Å correspond, respectively, to the lateral short-range order of the molten chains and the molecular cores confirming the liquid nature of the mesophase. The sharpness of the small-angle reflections indicates long-range correlation of the structure. However, these reflections do not conform to either a purely lamellar or purely columnar structure. The first three reflections (at 34.1, 17.1 and 11.4 Å) being in the reciprocal spacing ratio 1:2:3, point to a well-defined layered structure. In contrast the remaining two sharp reflections observed at 9.8 Å and 8.5 Å cannot be ascribed to a lamellar form, but can be explained by invoking a columnar ordering. Since these peaks are much less intense than the primary layer peak, they can be considered to be arising due to 2-D columnar modulation of the layers. A mesophase exhibiting structural features which is a combination of the lamellar and columnar features has been referred to as a lamello-columnar (Col_l) phase.[22,26,27,29] Symmetric 4-alkoxy substitituted Schiff base containing ethylene diamine spacer complexed to Pt^{2+}, Cu^{2+}, VO^{2+} and Ni^{2+} have also been shown to exhibit Col_l phases though the 1D ordering is more pronounced in these cases.[22,26,27,29] Though the corresponding Zn(II) complexes have been documented, the mesomorphic properties are not reported.[49] The low intensity for second wide-angle halo expected due to interaction between the rigid

part of one mesomorphic unit and its next nearest neighbour, suggests weaker correlation between the cores within the column in the mesophase. Enhanced flexibility associated with aliphatic spacer group bearing the 'methyl' substituent is believed to induce bending and twisting deformations, with the resulting fluctuations reducing the core-core correlations.[53,54] Similar behaviour has also been noticed for previously reported analogous salphen-Zn(II) and Cu(II) complexes with asymmetric methyl substituted aromatic spacer.[34,55]

The XRD spectrum recorded at 30°C (**Fig. 4.3b**) was quite similar to that recorded at high temperatures. However, the diffractogram consisted of additional reflections which agree with the assignment of the Col_l phase; the presence of diffuse reflections at wide angles and the absence of any mixed-index reflections at low angles rules out the phase to be crystalline in nature at this temperature. Further, the core-core peak becomes much stronger. Inserting the full width at half-maximum value of this reflection, in the standard Scherer equation yields a correlation length of about 115 Å, associated with the stacking of about 28 molecules along the columns. It may also be mentioned that the calculated inter-layer distance in the mesophase; d = 34.1Å, is greater than the DFT computed radius (~ 23.9Å) of the fully extended half-disc shaped molecule. Though additional information regarding the stacking of the molecular cores in the mesophase is not available, it is presumed that the half-disc shaped molecules might perhaps preferably arrange themselves in an anti-parallel partially interdigitated manner within the layer (**Fig. 4.4**).[53,54]

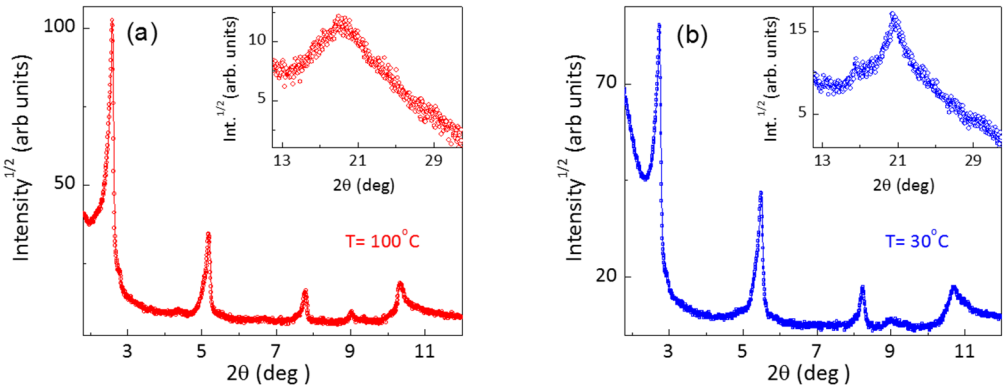

Fig. 4.3: PXRD pattern of **Zn-16dap** at (a) 100 °C and (b) at room temperature (30 °C).

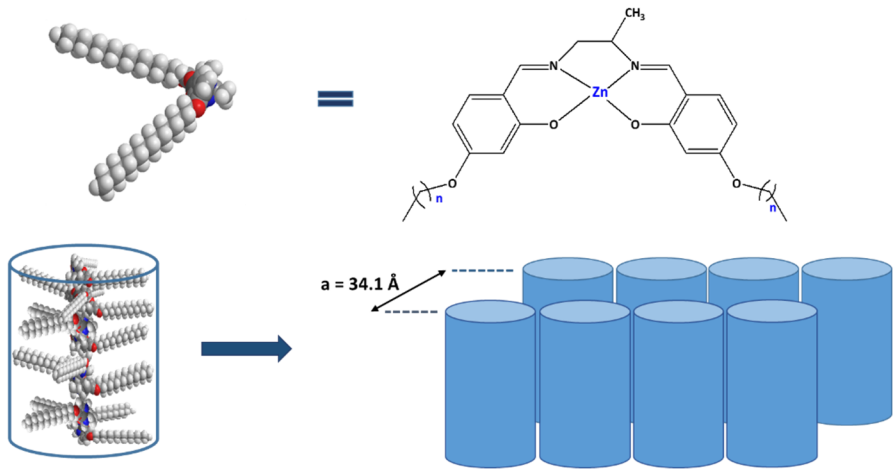

Fig. 4.4: Anti-parallel interdigitated organization of the molecules in lamello-columnar phase.

Table 4.2: PXRD data of **Zn-16dap**.

Temperature (°C)	Parameters	$d_{meas.}$/Å[a, b]	$d_{calc.}$/Å[a, b]	Miller indices(hkl)[c]
At 100 °C	a = 34.06 Å	34.05[s]	34.06	100
	b = 40.46 Å	17.06[s]	17.03	200
	V_{cell} =5540.5 Å^3	11.37[s]	11.35	300
	d = 34.1 Å	9.81[s]	9.70	140
		8.54[s]	8.70	240
		4.68[d]		
		4.02[d]		
At 30 °C	a = 32.18 Å	32.19[s]	32.18	100
	b = 41.31 Å	16.10[s]	16.09	200
	V_{cell} = 5596.5 Å^3	10.72[s]	10.73	300
	d = 32.18 Å	9.87[s]	9.83	140
		8.24[s]	8.26	050
		7.87[s]	7.90	410
		6.51	6.55	350
		5.72	5.76	450
		5.32	5.32	610
		4.29[d]		
		4.21[d]		

[a] $d_{meas.}$ and $d_{calc.}$ are the experimentally measured and calculated diffraction spacing, respectively.

[b] Intensity of the reflections: s; sharp peak, d: diffuse peak. The distances are given in Å. [c] [*hkl*] are the Miller indices of the reflections. For Col_l phase, $d = (\sum l d_{l00})/N_{l00}$ where N_{l00} is the number of reflections. V_{cell}, is the unit cell volume.

4.3.3. Photophysical properties

The UV-visible absorption and photoluminescence spectra of the compounds recorded in chloroform, $CHCl_3$ (2×10^{-5} M) at room temperature have been shown in **Fig. 4.5a** and **b** and the data are summarized in **Table 4.3**. The UV-visible absorption spectra of the ligands (**ndap**; n = 12, 14, 16) consisted of two intense absorption bands centered at ~ 278 and ~ 310nm, attributed to π-π* transition localized on the aromatic rings (Fig. 4.5a). Another less intense band at ~ 386 nm may be attributed to n– π* excitation of the C=N fragment. Upon complexation, former two bands were red-shifted to ~287 and ~ 329nm, respectively, with appearance of an additional shoulder at ~ 346 nm, while the low intensity band due to n–π* transition in the ligand disappeared because of the participation of the nitrogen's lone pair in coordination to the Zn^{2+} ion. The photoluminescence spectra of the ligands and Zn(II)-salen complexes were recorded at room temperature in $CHCl_3$ solution (2×10^{-5} M), mesophase and also in the solid state (**Fig. 4.5b**). The ligands are non-emissive. The solid state emission spectra of the complexes were recorded by placing a uniform powder sheet between two quartz plates. The complexes showed blue luminescence with emission maxima centered at ~ 424nm and emission quantum yield of ~ 23% (solution), and ~ 5% (solid) under UV irradiation (330nm). The observed fluorescence emission originates from metal-perturbed π-π* ligand-centered transitions. With respect to solution, the position of the emission maxima is virtually unaltered in the solid state. However, the emission intensity quenches substantially following closer association of molecular cores in the solid state as compared to the solution. In POM study, the mesophase of the Zn(II) complex that developed at 125 °C during the cooling cycle freezes into a glassy state persisting till ambient temperature enabling photoluminescence study in the mesophase ($\lambda_{max} \approx 425$ nm) as well. Similar studies in the frozen glassy state were made earlier for related complexes.[24] The emission energies are virtually unaffected in the solid, solution and in the mesophase (**Fig. 4.5b**).

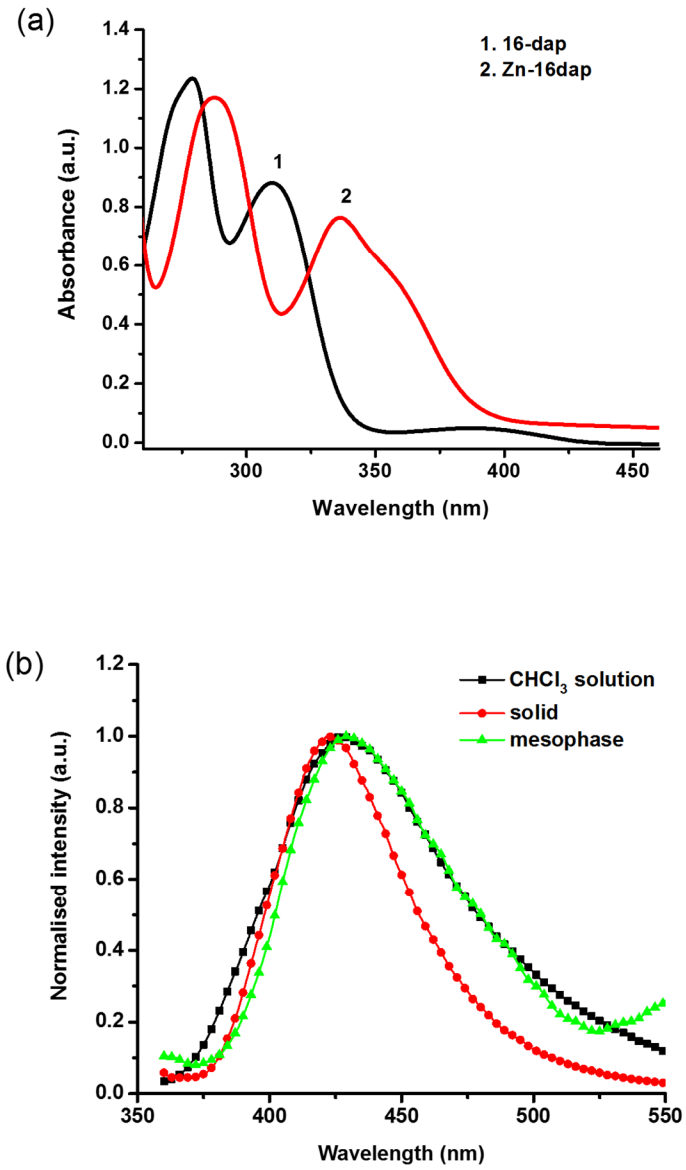

Fig. 4.5: (a) UV-visible absorption spectra of the **16dap** and **Zn-16dap** in chloroform (2×10^{-5} M) and (b) Intensity (normalized) vs. wavelength photoluminescence profile for **Zn-16dap** in chloroform solution (2×10^{-5}M), solid state and in mesophase ($\lambda_{ex.}$ = 330nm).

UV-visible and photoluminescence spectra of the Zn(II)-salen complexes (**Fig. 4.6a** and **b**) were also recorded in dilute solutions (2×10^{-5}M) of different coordinating and non-coordinating solvents in order to study the de-aggregation/ aggregation phenomena. The absorption spectra recorded in non-coordinating solvents (e.g. CH_2Cl_2, $CHCl_3$ and toluene) consisted of two well-defined bands located at ~ 287nm, 331nm and a shoulder at 345nm

(**Fig. 4.6a**) attesting formation of aggregates.[50,51] In coordinating solvent (THF), a red shift (~14nm) of the longer wavelength feature is observed due to the axial coordination of the solvent molecules, suggesting de-aggregation (**Fig. 4.6a**).[50,51] The coordinatively unsaturated Zn^{2+} ion behaves as a Lewis acid. This behaviour is unlike that observed in case of symmetrical molecule containing ethylenediamine spacer wherein upon de-aggregation; a blue shift of longer absorption feature was noticed.[49] A rather unusual optical behaviour is attributed to the lack of conjugation between the J-type aggregated 'salen' moieties. Methyl group being electron donating in nature induces a considerable amount of conjugation (+I effect) in the ligand framework in the present complexes. Also the tetrahedral methyl group due to its steric requirement tends to restrict salicylidene groups of each unit in the dimer to H-type aggregate (**Fig. 4.6c**). Similar results were obtained in other related systems with conjugated aliphatic and aromatic spacers.[50,51] Concentration variations had virtually no effect on these features up to a concentration of 1×10^{-4} M (**Fig. 4.7**). Photoluminescence spectra of the complexes (**Fig. 4.6b**) recorded in non-coordinating solvents exhibited a broad band at ~ 424nm. In coordinating solvents, the maxima is slightly red shifted (~8nm) with enhancement in fluorescent intensity suggesting de-aggregation with concomitant formation of 1:1 adduct.[50,51] The emission quantum yield values in non-coordinating solvents (e.g. CH_2Cl_2, $CHCl_3$ and toluene) are around 22% which were enhanced (EQY = 38%) upon de-aggregation in coordinating solvent. Fluorescence of face-to-face-stacked H-type dimer aggregates (sandwich-type dimers) are known to be quenched relative to that of the monomer.[56] A rapid energy relaxation of the lower excited states causes this fluorescence suppression. The absorption or emission characteristics of the complexes are invariant of the alkyl chain lengths (**Table 4.3**).

In order to minimize inter-electronic repulsions, Zn(II) ion prefers a tetrahedral geometry to a square planar coordination. However, a short rigid central spacer with steric demands in the present complexes forces the metal center to acquire unfavourable distorted planar geometry which eventually lead to a dimer, $[ZnL]_2$ [57] instead of more stable helical shape formed by tetrahedral 2:2 metal-to-ligand complex, $[Zn_2L_2]$.[58]

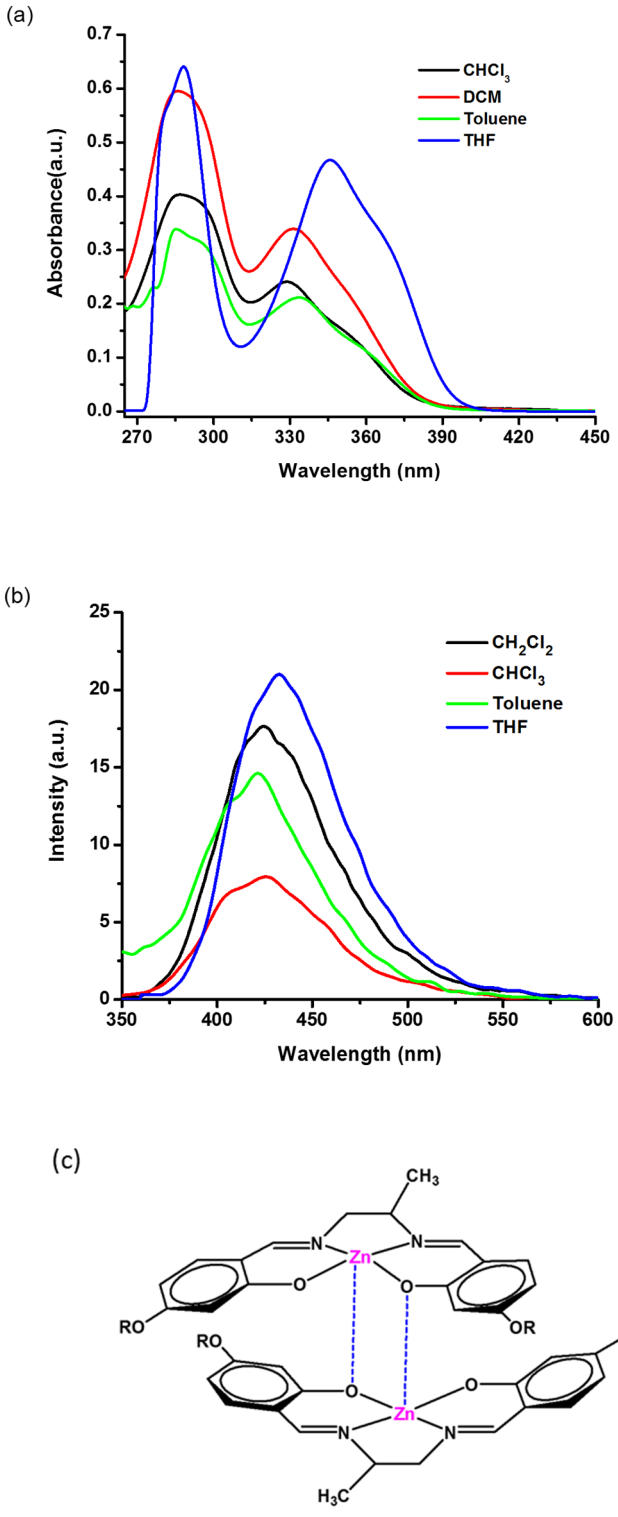

Fig. 4.6: UV-visible absorption spectra (a), fluorescence spectra ($\lambda_{ex.}$= 330nm; with 10% attenuator) (b) of **Zn-16dap** (2×10^{-5}M) in different non-coordinating and coordinating solvents and (c) the 'H-type' dimer in solution of non-coordinating solvents.

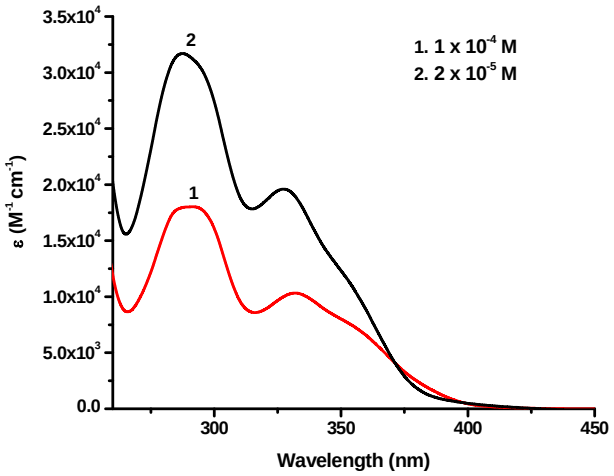

Fig. 4.7: Concentration dependence of UV-visible absorption spectra of **Zn-16dap** in $CHCl_3$ solutions.

Table 4.3: UV-visible and photoluminescence spectral data of the ligands (in $CHCl_3$) and **Zn-ndap** (n = 12, 14, 16) complexes in different solvents.

Compounds	Solvents	Absorption		Emission
		λ_{max}; nm	ε; l mol^{-1} cm^{-1}	λ_{max}; nm
12dap	$CHCl_3$	278, 310, 386	16,312, 12,300, 192	-
14dap	$CHCl_3$	278, 310, 386	15,936, 12,305, 200	-
16dap	$CHCl_3$	279, 310, 386	16,530, 12,296, 174	-
Zn-12dap	$CHCl_3$	287, 330, 345^{sh}	20,359, 11,240, 7,875	425
	CH_2Cl_2	286, 331, 345^{sh}	28,967, 16,543, 12,756	424
	Toluene	287, 333, 346^{sh}	16,748, 10,731, 8,156	421
	THF	288, 345, 360^{sh}	31,952, 23,675, 18,789	432
Zn-14dap	$CHCl_3$	287, 330, 347^{sh}	19,935, 10,306, 7,693	425
	CH_2Cl_2	286, 331, 347^{sh}	28,733, 16,238, 13,085	424
	Toluene	287, 333, 346^{sh}	16,892, 10,736, 9,712	422
	THF	288, 345, 361^{sh}	31,132, 22,925, 19,003	433
Zn-16dap	$CHCl_3$	287, 329, 343^{sh}	20,135, 10,240, 7,675	425
	CH_2Cl_2	286, 331, 346^{sh}	29,784, 16,998, 12,985	424
	Toluene	286, 333, 345^{sh}	16,998, 10,706, 8,215	421
	THF	288, 345, 359^{sh}	32,082, 23,405, 18,715	432

sh: shoulder

4.3.4. DFT study

In absence of diffraction quality single crystals, density functional theory (DFT) calculations were carried out on a representative Zn(II) complex (**Zn-16dap**) employing GAUSSIAN 09 program package[59] to ascertain the optimized electronic structure. The ground state geometry optimization in the gas phase of the zinc complex has been performed using the three-parameter fit of Becke's hybrid functional combined with the Lee-Yang-Parr correlation functional termed as B3LYP hybrid,[60,61] within generalized gradient approximation (GGA) exchange along with 6-311+G(d,p), 6-31+G(d,p), 6-31G(d) and 6-31G basis sets[62] for Zn, N, O, C and H, respectively, without imposing any symmetry constrain. Appropriate structure of the complex was confirmed as energy minima by calculating the vibrational frequency and confirming the absence of any imaginary frequencies. Based on the optimized geometry of the zinc complex, TD-DFT calculations on an isolated molecule of the title complex (**Zn-16dap**) have been performed at the B3LYP level to study the spectroscopic and electronic properties. Since the electronic absorption spectra of the compounds were recorded in dichloromethane, the solvent effects were taken into consideration in the theoretical modelling. GAUSSSUM[63] program was employed to calculate the individual contribution of various groups to each molecular orbital. A solvation method of the polarisable continuum model (PCM)[64] using the integral equation formalism (IEF) variant[65] were considered in calculations. Important geometric parameters of the optimized Zn(II) complex as evaluated by DFT at B3LYP level are collected in **Table 4.4**. Average Zn—O and Zn—N bond lengths of the Zn(II) complex are calculated to be 1.931 and 2.077Å, respectively. The O1–Zn–O2 and N1–Zn–N2 bond angles are found to be 108.9° and 80.0° respectively. The O1—Zn—N1, O2—Zn—N2, O1—Zn—N2 and O2—Zn—N1 bond angles are calculated to be 91.9°, 92.1°, 148.6° and 148.8°, respectively, around the zinc atom indicating a distorted square planar geometry (**Fig. 4.8**). The dihedral angle O1–N3–N2–O2 as evaluated from DFT calculation is about 39.7° reflecting a deviation from planarity.

The three-dimensional (3D) iso-surface plots of the lowest unoccupied molecular orbitals (LUMOs) and the highest occupied molecular orbitals (HOMOs) of the zinc complex are presented in **Fig. 4.9**. The electron density of the HOMO is localized almost entirely on the aromatic rings, while that of the LUMO is mainly centered on both N=C bonds and aromatic rings. The HOMO and LUMO energies are calculated to be −5.58 eV and −1.41 eV, respectively, the energy difference being ΔE = 4.17 eV. This value is somewhat higher than the HOMO–LUMO energy difference value (ΔE = 3.60 eV) evaluated from the lowest energy UV-Vis band (346nm). Extensive intermolecular interactions in the solution phase (UV-Vis study) as against a free gaseous molecule (DFT study) could be one plausible reason for such a deviation. While ligand p_π orbitals contribute almost entirely to HOMO-1(98%), HOMO-2(99%), HOMO-3(100%) orbitals, HOMO-4 orbital receives a negligible contribution from metal d_π orbitals(8%). Electron density on LUMO+1, LUMO+3 and LUMO+4 orbitals is mainly due to ligand p_π^* orbitals while that on LUMO+2 is primarily due to metal d_π^* orbitals(87%).

TD-DFT calculations have been carried out for the **Zn-16dap** complex to account for the observed bands in the UV-visible region. The key electronic transitions, corresponding oscillator strength (*f*), orbitals involved in these transitions and their percentage contribution to each transition are summarized in **Table 4.5**. The surface of each peak in the spectra is proportional to oscillator strength (*f*), which also reveals the probability of electronic transition. The title complex exhibits three absorption bands at 345, 336 and 295nm, respectively. The absorption band at 345nm corresponds to HOMO→LUMO electronic transition owing to the $L(\pi)\rightarrow L(\pi^*)$, where HOMO corresponds to π bonding orbitals of aromatic rings of the ligand and LUMO corresponds to π^* (anti-bonding) orbitals of the aromatic rings (intra-ligand charge transfer). This transition is consistent with the experimental value of 346nm. The high energy absorption bands of the complex occur at 336 and 295nm, which could be assigned to HOMO-1→LUMO and HOMO-2→LUMO electronic transitions, predominantly due to intra-ligand ($\pi\rightarrow\pi^*$) charge transfer. These two transitions resemble the experimental value of 331 and 286nm, respectively.

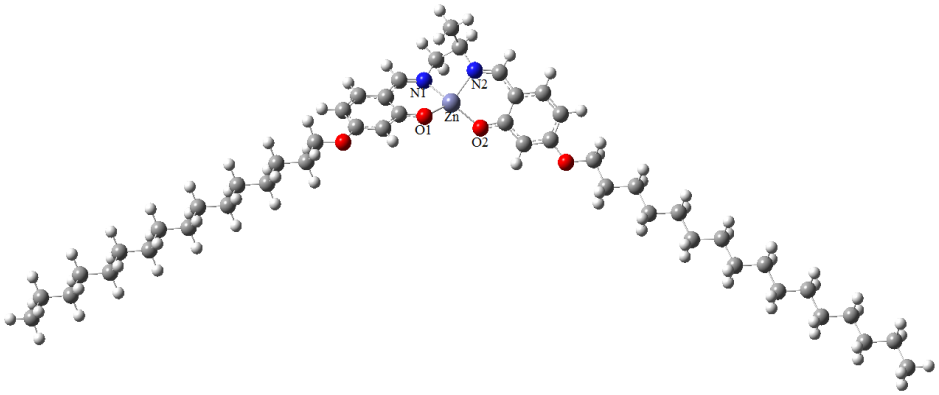

Fig. 4.8: DFT optimized structure of a representative complex, **Zn-16dap**.

Table 4.4: Selected bond lengths (Å) and bond angles (°) of **Zn-16dap** optimized at the B3LYP level.

Structural parameters	**Bond Lengths (Å) and Bond angles (°)**
Zn—O1	1.932
Zn—O2	1.931
Zn—N1	2.076
Zn—N2	2.078
O1—Zn—O2	108.9
N1—Zn—N2	80.0
O1—Zn—N1	91.9
O2—Zn—N2	92.1
O1—Zn—N2	148.6
O2—Zn—N1	148.8
O1—N1—N2—O2	39.7
Molecular length	47.8

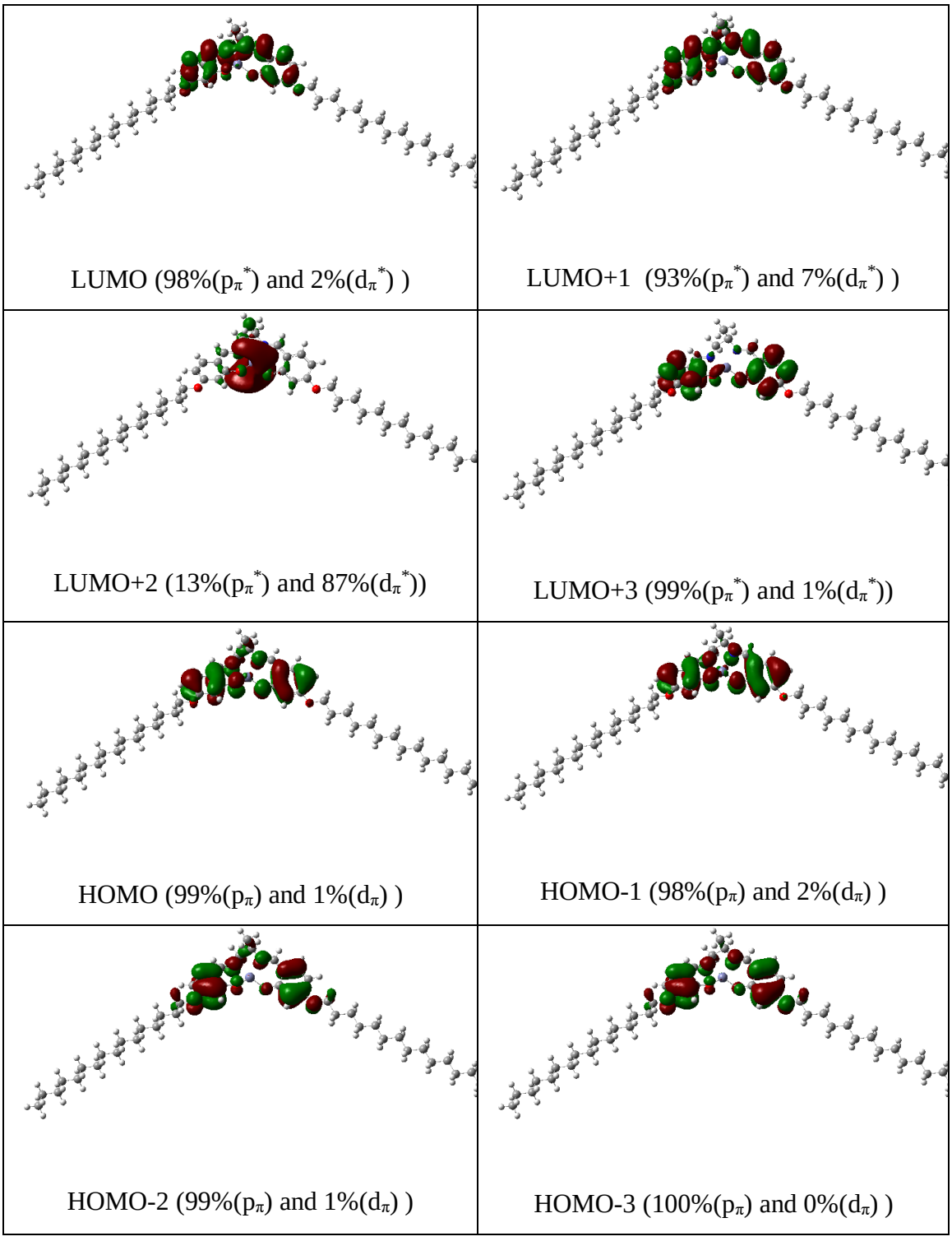

Fig. 4.9: Frontier molecular orbitals of **Zn-16dap**.

Table 4.5: The experimental absorption bands and the electronic transitions calculated with TD-DFT/B3LYP method of the **Zn-16dap** complex.

Key transition	Character	λ (nm)	E (eV)	*f* (Osc. Strength)	Assignments	λ_{exp}(nm) ε($lmol^{-1}cm^{-1}$)
(90%)HOMO→LUMO	L(π)→L(π*)	345	3.60	0.124	IL	346 (12,985)
(89%)HOMO-1→LUMO	L(π)→L(π*)	336	3.70	0.102	IL	331 (16,998)
(85%) HOMO-2→LUMO	L(π)→L(π*)	295	4.21	0.550	IL	286 (29,784)

4.4. Conclusion

A series of new Zn(II) complexes of 'salen' type asymmetric Schiff base ligands bearing long pendant alkoxy arm at the 4-position of side aromatic rings and an asymmetric central spacer group have been accessed. Co-ordination of Zn^{2+} ion to the ligands induces lamello-columnar mesomorphism in otherwise non-mesomorphic ligands. These half-disc shaped molecules assemble in an anti-parallel interdigitated manner within the layer in the mesophase. Metal coordination also brings about interesting fluorescent properties in solid state, solution and as well as in the mesophase. In addition, the complexes also exhibit aggregation behaviour in dilute solutions of different non-coordinating and coordinating solvents suggesting the Lewis acidity of the metal ion in the newly synthesized complexes. Asymmetric methyl substitution at the aliphatic spacer leads to variation in photophysical behaviour and mesophase order in the present complexes as compared to symmetric molecules containing ethylenediamine spacer. The coordinative unsaturation of Zn(II)-complexes may be utilized for binding other suitable donor groups to tune the properties.

REFERENCES

[1] A.W. Kleij, *Eur. J. Inorg. Chem.*, 2009, 193.

[2] A.W. Kleij, *Chem. Eur. J.*, 2008, **14**, 10520.

[3] S. J. Wezenberg, A.W. Kleij, *Angew. Chem. Int. Ed.*, 2008, **47**, 2354.

[4] G. H. Clever, T. Carell, *Angew. Chem. Int. Ed.*, 2007, **46**, 250.

[5] K. C. Gupta, A. K. Sutar, *Coord. Chem. Rev.*, 2008, **252**, 1420.

[6] P. G. Cozzi, *Chem. Soc. Rev.*, 2004, **33**, 410.

[7] L. Canali, D. C. Sherrington, *Chem. Soc. Rev.*, 1999, **28**, 85.

[8] E. N. Jacobsen, *in Catalytic Asymmetric Synthesis, ed. I. Ojima, VCH, New York*, 1993, pp. 159.

[9] G. Barone, N. Gambino, A. Ruggirello, A. Silvestri, A. Terenzi, V. T. Liveri, *J. Inorg. Biochem.*, 2009, **103**, 731.

[10] Y. Kou, J. Tian, D. Li, W. Gu, X. Liu, S. Yan, D. Liao, P. Cheng, *Dalton Trans.*, 2009, 2374.

[11] A. Silvestri, G. Barone, G. Ruisi, D. Anselmo, S. Riela, V. T. Liveri, *J. Inorg. Biochem*., 2007, **101**, 841.

[12] C. Liu, M. Wang, T. Zhang, H. Sun, *Coord. Chem. Rev.*, 2004, **248**, 147.

[13] J. Cheng, K. Wei, X. Ma, X. Zhou, H. Xiang, *J. Phys. Chem. C.*, 2013, **117**, 16552.

[14] V. Liuzzo, W. Oberhauser, A. Pucci, *Inorg. Chem. Commun.*, 2010, **13**, 686.

[15] H.-C. Lin, C.-C. Huang, C.-H. Shi, Y.-H. Liao, C.-C. Chen, Y.-C. Lin, Y.-H. Liu, *Dalton Trans.*, 2007, 781.

[16] E. Hadjoudis, I. M. Mavridis, *Chem. Soc. Rev.*, 2004, **33**, 579.

[17] M. Andruh, *Chem. Commun.*, 2011, **47**, 3025.

[18] H. Miyasaka, A. Saitoh, S. Abe, *Coord. Chem. Rev.*, 2007, **251**, 2622.

[19] I. P. Oliveri, S. Failla, A. Columbo, C. Dragonetti, S. Righetto, S. Di Bella, *Dalton Trans.*, 2014, **43**, 2168.

[20] S. Di Bella, I. P. Oliveri, A. Colombo, C. Dragonetti, S. Righetto, D. Roberto, *Dalton Trans.*, 2012, **41**, 7013.

[21] P. G. Lacroix, *Eur. J. Inorg. Chem.*, 2001, 339.

[22] Y. Abe, Y. Takagi, M. Nakamura, T. Takeuchi, T. Tanase, M. Yokokawa, H. Mukai,

T. Megumi, A. Hachisuga, K. Ohta, *Inorg. Chim. Acta*, 2012, **392**, 254.

[23] A. Ohta, Y. Yamamoto, H. Kamihata, Y. H. Lee, F. Ichikawa, K. Ohta, Y. Abe, N. Hoshino, M. Kojima, S. Hayami, *Inorg. Chem. Commun.*, 2012, **16**, 89.

[24] D. Pucci, I. Aiello, A. Bellusci, A. Crispini, M. Ghedini, M. La Deda, *Eur. J. Inorg. Chem.*, 2009, 4274.

[25] I. Aiello, A. Bellusci, A. Crispini, M. Ghedini, D. Pucci, T. Spataro, *Mol. Cryst. Liq. Cryst.*, 2008, **481**, 1.

[26] Y. Abe, N. Nakazima, T. Tanase, S. Katano, H. Mukai, K. Ohta, *Mol. Cryst. Liq. Cryst.*, 2007, **466**, 129.

[27] Y. Abe, K. Nakabayashi, N. Matsukawa, H. Takashima, M. Iida, T. Tanase, M. Sugibayashi, H. Mukai, K. Ohta, *Inorg. Chim. Acta*, 2006, **359**, 3934.

[28] K. Binnemans, K. Lodewyckx, T. Cardinaes, T. N. Parac Vogt, C. Bourgogne, D. Guillon, B. Donnio, *Eur. J. Inorg. Chem.*, 2006, 150.

[29] Y. Abe, H. Akao, Y. Yoshida, H. Takashima, T. Tanase, H. Mukai, K. Ohta, *Inorg. Chim. Acta*, 2006, **359**, 3147.

[30] L. L. Li, H. F. Xiang, X. G. Zhou, M. L. Li, D. Wu, *J. Chem. Educ.*, 2012, **89**, 559.

[31] V. K. Gupta, R. N. Goyal, A. K. Jain, R. A. Sharma, *Electrochim. Acta*, 2009, **54**, 3218.

[32] V. K. Gupta, A.K. Jain, G. Maheshwari, *Talanta*, 2007, **72**, 49.

[33] C. R. Bhattacharjee, G. Das, P. Mondal, S. K. Prasad, D.S.S. Rao, *Eur. J. Inorg. Chem.*, 2011, 1418.

[34] C. R. Bhattacharjee, G. Das, P. Mondal, N.V.S. Rao, *Polyhedron*, 2010, **29**, 3089.

[35] I. P. Oliveri, S. Di Bella, *Tetrahedron*, 2011, **67**, 9446.

[36] M. E. Germain, M. J. Knapp, *J. Am. Chem. Soc.*, 2008, **130**, 5422.

[37] M. E. Germain, T. R. Vargo, P. G. Khalifah, M. J. Knapp, *Inorg. Chem.*, 2007, **46**, 4422.

[38] M. Cano, L. Rodríguez, J. C. Lima, F. Pina, A.D. Cort, C. Pasquini, L. Schiaffino, *Inorg. Chem.*, 2009, **48**, 6229.

[39] A. D. Cort, L. Mandolini, C. Pasquini, K. Rissanen, L. Russo, L. Schiaffino, *New J. Chem.*, 2007, **31**, 1633.

[40] S. J. Wezenberg, E. C. Escudero-Adán, J. Benet-Buchholz, A.W. Kleij,

Inorg. Chem., 2008, **47**, 2925.

[41] A.W. Kleij, M. Kuil, D. M. Tooke, A. L. Spek, J. N. H. Reek, *Inorg. Chem.*, 2007, **46**, 5829.

[42] M. Kuil, I. M. Puijk, A. W. Kleij, D. M. Tooke, A. L. Spek, J. N. H. Reek, *Chem.–As. J.*, 2009, **4**, 50.

[43] A. W. Kleij, M. Kuil, D. M. Tooke, M. Lutz, A. L. Spek, J. N. H. Reek, *Chem. Eur. J.*, 2005, **11**, 4743.

[44] M. Kuil, P. E. Goudriaan, A. W. Kleij, D. M. Tooke, A. L. Spek, P. W. N. M. van Leeuwen, J. N. H. Reek, *Dalton Trans.*, 2007, 2311.

[45] P. G. Cozzi, *Angew. Chem.*, 2003, **115**, 3001.

[46] A. A. Vashchenko, L. S. Lepnev, A. G. Vitukhnovskii, O. V. Kotova, S. V. Eliseeva, N. P. Kuźmina, *Opt. Spectrosc.*, 2010, **108**, 463.

[47] O. V. Kotova, S. V. Eliseeva, A. S. Averjushkin, L. S. Lepnev, A. A. Vaschenko, A.Y. Rogachev, A. G. Vitukhnovskii, N. P. Kuzmina, *Russ. Chem. Bull. Int. Ed.*, 2008, **57**, 1880.

[48] K. H. Chang, C. C. Huang, Y. H. Liu, Y. H. Hu, P. T. Chou, Y. C. Lin, *Dalton Trans.*, 2004, 1731.

[49] G. Consiglio, S. Failla, P. Finocchiaro, I. P. Oliveri, S. Di Bella, *Inorg. Chem.*, 2012, **51**, 8409.

[50] G. Consiglio, S. Failla, P. Finocchiaro, I. P. Oliveri, S. Di Bella, *Dalton Trans.*, 2012, **41**, 387.

[51] G. Consiglio, S. Failla, I.P. Oliveri, R. Purrello, S. Di Bella, *Dalton Trans.*, 2009, 10426.

[52] A. W. Kleij, *Dalton Trans.*, 2009, 4635.

[53] A. G. Serrette, C. K. Lai, T. M. Swager, *Chem. Mater.*, 1994, **6**, 2252.

[54] S. T. Trzaska, T. M. Swager, *Chem. Mater.*, 1998, **10**, 438.

[55] C. Datta, R. Chakrabarty, G. Das, C. R. Bhattacharjee, P. Mondal, *Liq. Cryst.*, 2013, **41**, 541.

[56] M. Kasha, H. R. Rawls, M. A. El-Bayoumi, *Pure Appl. Chem.*, 1965, **11**, 371.

[57] G. E. Batley, D. P. Graddon, *Aust. J. Chem.*, 1967, **20**, 885.

[58] S. Mizukami, H. Houjou, Y. Nagawa, M. Kanesato, *Chem. Commun.*, 2003, 1148.

[59] M. J. Frisch, G. W. Trucks, H. B. Schlegel, G. E. Scuseria, M. A. Robb, J. R. Cheeseman, G. Scalmani, V. Barone, B. Mennucci, G. A. Petersson, H. Nakatsuji, M. Caricato, X. Li, H. P. Hratchian, A. F. Izmaylov, J. Bloino, G. Zheng, J. L. Sonnenberg, M. Hada, M. Ehara, K. Toyota, R. Fukuda, J. Hasegawa, M. Ishida, T. Nakajima, Y.Honda, O. Kitao, H. Nakai, T. Vreven, J. A. Montgomery Jr., J. E. Peralta, F. Ogliaro, M. Bearpark, J. J. Heyd, E. Brothers, K. N. Kudin, V. N. Staroverov, R. Kobayashi, J. Normand, K. Raghavachari, A. Rendell, J. C. Burant, S. S. Iyengar, J. Tomasi, M. Cossi, N. Rega, J. M. Millam, M. Klene, J. E. Knox, J. B. Cross, V. Bakken, C. Adamo, J. Jaramillo, R. Gomperts, R. E. Stratmann, O. Yazyev, A. J. Austin, R. Cammi, C. Pomelli, J. W. Ochterski, R. L. Martin, K. Morokuma, V. G. Zakrzewski, G. A. Voth, P. Salvador, J. J. Dannenberg, S. Dapprich, A. D. Daniels, Ö. Farkas, J. B. Foresman, J.V. Ortiz, J. Cioslowski, D. J. Fox, GAUSSIAN 09, Gaussian Inc., Wallingford CT, 2009.

[60] A. D. Becke, *J. Chem. Phys.*, 1993, **98**, 5648.

[61] C. Lee, W. Yang, R. G. Parr, *Phys. Rev. B*, 1988, **37**, 785.

[62] P.C. Hariharan, J. A. Pople. *Theor. Chim. Acta*, 1973, **28**, 213.

[63] N. M. O'Boyle, A. L. Tenderholt, K. M. Langner, *J. Comput. Chem.*, 2008, **29**, 839.

[64] E. Cance, B. Mennucci, J. Tomasi, J. Chem. Phys., 1997, **107**, 3032.

[65] S. Miertus, E. Scrocco, J. Tomasi, *J. Chem. Phys.*, 1981, **55**, 117.